



Enhancing cycling performance of FeF₃ cathode by introducing a lightweight high conductive adsorbable interlayer



Xiangyang Zhou^a, Hongxu Sun^a, Haochen Zhou^b, Zhanglin Xu^a, Juan Yang^{a,*}

^a School of Metallurgy and Environment, Central South University, Changsha, 410083, China

^b Department of Aerospace, Tsinghua University, Beijing, 100084, China

ARTICLE INFO

Article history:

Received 15 February 2017

Received in revised form

18 June 2017

Accepted 24 June 2017

Available online 27 June 2017

Keywords:

Iron fluoride

Porous hollow carbon nanofiber

Interlayer

Electrode pulverization

Cathodes

ABSTRACT

Iron fluorides, as a kind of high specific capacity conversion-type cathode materials for lithium rechargeable batteries, are attracting an increasing number of researchers. However, their practical applications are hindered by the poor electrical conductivity and the volume effect during cycling. In this work, a lightweight porous hollow carbon nanofiber (PHCNF) interlayer is proposed to coat on the original FeF₃ cathode to solve these problems. This interlayer is synthesized through a facile carbonizing-activating process using polypyrrole (PPy) as raw material, and plays a difunctional role in trapping the escaped FeF₃ particles and improving the electrical conductivity of electrode. By introducing the high conductive coating layer, an extremely high specific capacity of 217 mAh g⁻¹ for 40 cycles in the 2–4.5 V region is achieved, which is close to the theoretical specific capacity of 237 mAh g⁻¹ for FeF₃. Also, a superior power capability is retained delivering a reversible specific capacity of 193 mAh g⁻¹ at 200 mA g⁻¹ and 101 mAh g⁻¹ even at 1000 mA g⁻¹.

© 2017 Elsevier B.V. All rights reserved.

1. Introduction

Recently, with the vigorous development of portable electronic devices, lithium rechargeable batteries are now considered as one of the dominant power sources for a variety of electric storage applications due to their high storage capacity, and long cycle life [1–3]. However, current state-of-the-art Li-ion batteries could not satisfy the fast-growing demand for higher specific capacity, power density and safety. To further improve the performance of lithium ion batteries, the research for new type electrode material, especially cathode materials, for Li-ion batteries has been highlighted. The theoretical capacity of traditional cathode materials (such as LiFePO₄, LiCoO₂) is often low (140–170 mAh g⁻¹), because of the intercalation reactions based on single or less electron reaction [4,5]. Accordingly, an effective strategy for high capacity electrodes is to utilize conversion reaction with multi-electron transfer [6–15]. during the conversion reactions, phase transitions occur with the general equation as follows: MX_m + nLi ↔ M + nLiX_{m/n}, where M is transition metal, X is anion.

Among kinds of the conversion-type compounds, metal

fluorides such as NiF₂ with an average discharge charge voltage of 2.96 V and a theoretical specific capacity of 554 mAh g⁻¹ [16], CoF₂ (2.85 V, 553 mAh g⁻¹) [17], CuF₂ (3.55 V, 528 mAh g⁻¹) [18,19], FeF₂ (2.66 V, 571 mAh g⁻¹) [20,21], FeF₃ (2.74 V, 712 mAh g⁻¹) [22,23], etc have been investigated as cathode materials for Li-ion batteries, owing to their high operating voltages and high theoretical specific capacities. A representative example is iron trifluoride (FeF₃), the electrochemical reaction mechanism of which was proposed by Badway [24–26], which can be described as a two-step reaction. With the initial insertion of Li⁺, the intercalated “LiFeF₃” is formed. A first voltage plateau is around 3.4 V, and then the second plateau of around 2.1 V appears with the conversion reaction producing Fe and LiF. These two step reactions involve three-electron transfer, so it is generally acknowledged that FeF₃ has a high theoretical specific capacity of 237 mAh g⁻¹ (one-electron transfer) testing between 2.0 and 4.5 V, this voltage range is similar to some other high capacity conversion-type cathode materials, such as vanadium oxides [27,28]. Furthermore, a larger theoretical specific capacity of 712 mAh g⁻¹ (three-electron transfer) can be achieved testing between 1.5 V and 4.5 V region [29–32]. Moreover, the peculiarities of low toxicity, low cost and better cyclability than other metal fluorides, make FeF₃ a very promising candidate of the cathode materials for Li-ion batteries.

Nevertheless, several drawbacks, such as high ionicity and poor

* Corresponding author.

E-mail address: jyang_csu@163.com (J. Yang).

structural stability, prevent FeF_3 from its practical application as a cathode material. The high ionicity of FeF_3 induces a large band gap, thus FeF_3 , like most metal fluorides, invariably exhibits insulating behavior, giving rise to large hysteresis voltage, poor cycling and rate capability. What is worse, the pulverization of electrodes, resulting from the large volume effect accompany with the structural changes during battery operation, severely degrades the cyclability of the conversion-type FeF_3 cathode [20]. To address the above-mentioned issues, various measures were taken, which could be mainly summed up in three aspects: i) Rational morphologies designing and nanocrystallization of FeF_3 . Rational designed morphologies could alleviate the volume effect and shorten the ion transport path, while nanoscaled crystallite dimension could significantly improve the reaction activity of the FeF_3 particles. For example, Ma et al. prepared a three-dimensionally ordered macroporous FeF_3 hybrid structure which delivered a reversible capacity of 190 mAh g^{-1} for 30 cycles at 20 mA g^{-1} [22]. ii) Fabrication of FeF_3 based composite with conductive carbonaceous materials [23,33]. The building of the carbonaceous conductive framework could effectively improve the cyclability and rate performance of the composite materials. Kim et al. fabricated FeF_3 nanoflowers on CNT branches, sustained a reversible capacity of nearly 200 mA g^{-1} for 30 cycles at 20 mA g^{-1} [23]; Liu et al. synthesized uniform iron fluoride nanocrystals on reduced graphene oxide sheets, a capacity of 205 mA g^{-1} for 30 cycles at 45 mA g^{-1} was achieved [33]. iii) Element doping. Smaller band gap can improve the electronic conductivity of FeF_3 itself and alleviate the sluggish kinetics of FeF_3 , in addition, doping element can effect microcrystal growth. For example, Bai et al. prepared $\text{Fe}_{(1-x)}\text{Ti}_x\text{F}_3$ by a hydrothermal method, which retained the specific capacity of 174 mAh g^{-1} at 23.7 mA g^{-1} [34]. Overall, a majority of research focus on the fabrication of FeF_3/C composite to modify the cyclability and rate performance of FeF_3 , and some good results are achieved. But the current resulting reversible capacities are not satisfactorily high, and the cycle performance still need to be improved, which may be partially responsible for the pulverization phenomenon of FeF_3 based composite cathodes, since it still exists in the case of low carbon content.

Considering that the electrode pulverization is difficult to avoid for conversion-type cathode materials. A macroscopic electrode structure was designed by introducing an interlayer inserted between electrode and separator by our group [35], and an excellent performance was achieved which retained an ultrahigh capacity of 600 mAh g^{-1} at 100 mA g^{-1} for 60 cycles. Unfortunately, the proportion of interlayer in electrode remains to be further reduced. In this work, a lightweight conductive interlayer between active material and separator is designed to apply to conversion-type cathode materials, simply by coating the surface of FeF_3 cathode with a porous hollow carbon nanofiber (PHCNF) film directly. The coating film is thick in order to ensure a high proportion of active material, which accounted for only 27.9 wt% of the whole cathode (cathode layer and interlayer). A schematic illustration of the designed cell configuration and the preparation process of PHCNF are shown in Scheme 1. The PHCNF can be synthesized through a facile carbonizing-activating process using PPy as raw material. The as-synthesized PHCNF possesses a three dimensional cross-linked network structure with a large specific surface area, which comes from the porous hollow structure of every carbon fiber. The hollow structure can reduce the weight of the interlayer, and the highly porous structure can provide abundant accommodate space for the escaped FeF_3 nanoparticles also benefit the electrolyte permeation. The cross-linked conductive carbon network plays a key role in stabilizing the electrode structure and reducing the internal resistance of the battery simultaneously. Thus the “double-layer” electrode configuration provides an effective way to resolve the

problems of volume effect and electrode pulverization, from which most conversion-type electrodes are suffering [36].

The application of the carbon nanofiber interlayer enables the pure FeF_3 cathode to retain an extremely high reversible specific capacity of 217 mAh g^{-1} after 40 cycles at 20 mA g^{-1} , which is close to the theoretical specific capacity of 237 mAh g^{-1} of FeF_3 . The specific energy is also retained at more than 612 Wh kg^{-1} under these conditions. To the best of our knowledge, this is the highest specific capacity and energy among the ever published results under the same test conditions. Interestingly, the composite cathode also deliver an excellent rate performance, reversible capacities of 193 mAh g^{-1} , 174 mAh g^{-1} and 101 mAh g^{-1} are achieved at 200 mA g^{-1} , 400 mA g^{-1} and 1000 mA g^{-1} , respectively. It should be noted that the outstanding performance of the novel design of electrode configuration may well prove the possibility of conversion-type compounds being used as commercial electrode materials for Li rechargeable batteries.

2. Experimental

2.1. Synthesis of iron fluoride (FeF_3)

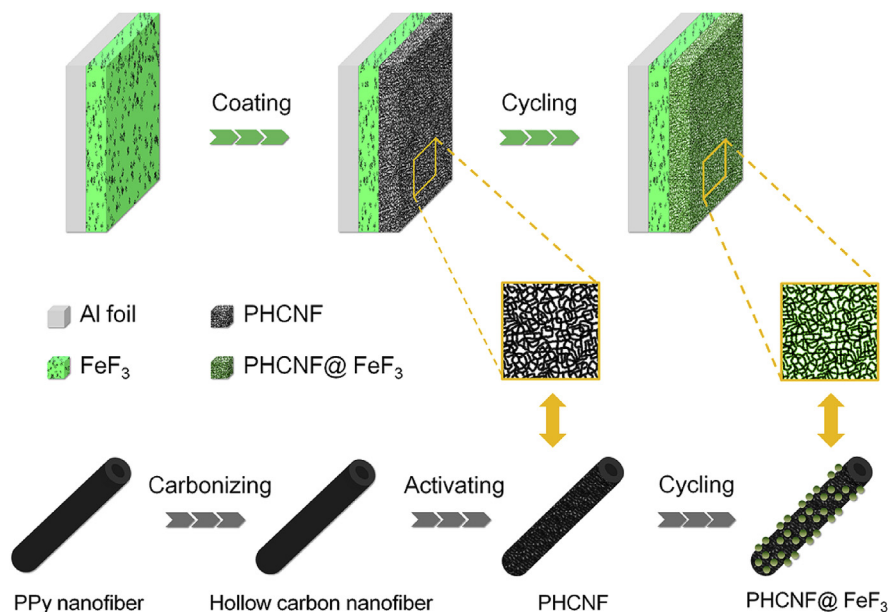
FeF_3 powders were synthesized by a facile liquid-phase method. Firstly, 70 mL FeCl_3 (0.02 M) ethanol solution was prepared in Teflon-lined autoclave, then, 30 mL HF solution (40%) was added into FeCl_3 ethanol solution dropwise, after stirring, the bright yellow solution gradually became colorless. After another stirring for 0.5 h , the Teflon-lined autoclave was sealed and heated in an oven at $60 \text{ }^\circ\text{C}$ for 10 h . The generated pink precipitate was collected and washed with absolute ethanol for several times, following by drying at $80 \text{ }^\circ\text{C}$ for 8 h to get $\text{FeF}_3 \cdot 3\text{H}_2\text{O}$ powders as precursor. After another drying at $120 \text{ }^\circ\text{C}$ for 48 h , the FeF_3 light green powders were obtained.

2.2. Synthesis of the PHCNF

The porous hollow carbon nanofiber was prepared from polypyrrole nanofiber. The polypyrrole nanofiber was synthesized by our previous work [37,38]. Briefly, 7.3 g CTAB and 13.7 g ammonium persulfate was dissolved in 120 mL HCl solution (1 M), respectively. After stirring in ice bath for 0.5 h , a white reactive template was achieved. Then, 8.3 mL pyrrole monomer was added slowly, the black precipitate was obtained after 24 h stirring at $0\text{--}5 \text{ }^\circ\text{C}$. After collecting and washing for several times with deionized water and absolute ethanol, the black precipitate was during at $80 \text{ }^\circ\text{C}$ in an oven for 12 h . Then, the as-synthesized polypyrrole nanofiber was heated at $700 \text{ }^\circ\text{C}$ for 2 h under a N_2 atmosphere for carbonization. The as-obtained carbon nanofiber and KOH were mixed with a mass ratio of $3:1$ in ethanol and deionized water mixed solution. After drying, the mixture was heated at $700 \text{ }^\circ\text{C}$ for 1 h in N_2 atmosphere for activation, and then the product was washed to ensure that the chloride ions was removed completely. Finally, the porous hollow carbon nanofiber (PHCNF) doped with nitrogen were obtained after drying in an oven overnight at $80 \text{ }^\circ\text{C}$.

2.3. Materials characterization

The phases of the synthesized materials were characterized by transmission electron microscopy (TEM, JEM-2100F, Japan), scanning electron microscope (SEM, Nova NanoSEM230, USA), and X-ray diffraction (XRD, Rigaku-TTRIII, Japan). Elemental analysis was made by an energy dispersive spectrometer (EDS). The pore diameter distribution, total pore volume and specific surface area were identified through a Surface Area and Porosity Analyzer (ASAP 2020HD88, USA). Digital photos were taken with a digital camera



Scheme 1. A schematic of electrode configuration and the preparation process of porous hollow carbon nanofiber (PHCNF).

(CASIO EX-ZR400, Japan). Surface elemental analysis was carried out by using an X-ray photoelectron spectrometer (XPS, K-Alpha 1063, USA).

2.4. Electrode preparation and electrochemical measurements

The iron fluoride cathode was made by mixing 20% acetylene black, 10% polyvinylidene fluoride (PVDF) and 70% pure FeF_3 in *N*-methyl-2-pyrrolidinone (NMP). The well mixed slurry was coated on aluminum foil and dried at 120 °C overnight in a vacuum oven. As for the preparation of the “double-layer” cathode, the slurry of carbon nanofiber was produced by mixing 95% PHCNF and 5% polyvinylidene fluoride (PVDF), followed by coating onto as-dried iron fluoride cathode with a scraper blade and drying at 120 °C for another 12 h. The electrodes were cut into pellets of 1.0 cm in diameter, and the coin cells were assembled with Li metal foil as the anode in an argon-filled glove box (Super 1220/750, Shanghai Mikrouna Co. Ltd.). A Celgard 2400 polypropylene membrane was served as the separator. LiPF_6 (1 M) in ethylene carbonate (EC) and diethyl carbonate (DEC) with a volume ratio of 1: 1 as the electrolyte. The cells were tested in voltage ranges of 4.5–2.0 V and 4.5–1.5 V (~vs. Li/Li^+) at different current densities of 20–1000 mA g^{-1} on a LAND CT-2001A (Wuhan, China). Cyclic voltammograms (CV) were measured by an electrochemical workstation (PARSTAT 4000, USA) at a scanning rate of 0.1 mV s^{-1} in voltage ranges of 4.5–2.0 V and 4.5–1.5 V. Also, electrochemical impedance spectra (EIS) were obtained by PARSTAT 4000 electrochemical workstation from 100 kHz to 10 mHz with an automatic scanning mode.

3. Results and discussion

Anhydrous FeF_3 possesses a hexagonal lattice belonging to the R-3c space group, which is described to have a ReO_3 type structure with the lattice parameter values of a (5.20 Å), b (5.20 Å), c (13.32 Å) and V (311.99 Å³), and this structure is larger than other similar type structure, such as TiOF_2 and Nb_2OF [6]. FeF_3 has a number of hydrated structures, and kinds of them have been studied as cathode materials by researchers, such as $\text{FeF}_3 \cdot 3\text{H}_2\text{O}$, $\text{FeF}_3 \cdot 0.5\text{H}_2\text{O}$

and $\text{FeF}_3 \cdot 0.33\text{H}_2\text{O}$ [39–41]. Water molecules act as structural stabilizers during the electrochemical reaction, but limit the theoretical capacity partly and are likely to bring about the side reaction with LiPF_6 in the electrolyte. Usually, it is difficult to obtain the anhydrous FeF_3 , because Fe_2O_3 is often detected while removing the water of crystallization from hydrated ones through the high temperature heat treatment. In this study, anhydrous FeF_3 were synthesized through a facile liquid-phase method and subsequent mild heat treatment. The X-ray diffraction (XRD) pattern of the as-synthesized FeF_3 powders is clearly represented in Fig. 1a. As is shown, all XRD peaks of the as-synthesized powders are identified as FeF_3 (JCPDS 33-0647), crystallizing in a ReO_3 -type structure with a space group of R-3c, no other impurity signal is detected in XRD pattern. The widened peaks are mainly associated with the removal of crystal water under heat treatment, which leads to an amorphous characteristic of the corresponding XRD peaks.

The morphology of FeF_3 is shown in Fig. 1b–d, a regular spindle-shaped morphology of FeF_3 particles is observed with an average length of 10–50 μm . Interestingly, it can be found that a few spindle-shaped FeF_3 particles agglomerate into a radiated aggregate. As shown from the TEM image of FeF_3 in Fig. 1d. The as-synthesized FeF_3 is a kind of typical micro-nano structure. Although the grain size of the FeF_3 particles observed from SEM image is relatively huge, the spindle-shaped particles are composed of primary nanoparticles with diameter of only about 20 nm. The primary nanoparticles can improve the reaction activity of FeF_3 , and the gaps between them are expected to increase the contact area with the electrolyte.

However, for pure FeF_3 electrode, the structural collapse of the FeF_3 particles is difficult to avoid in subsequent cycling. The high conductive cross-linked carbon network interlayer composing of PHCNF can solve this issue well. Typical SEM and TEM images of PHCNF are shown in Fig. 2a–b, the as-obtained PHCNF shows clearly homogeneous morphology of cross-linked hollow nanofibers with external diameter of about 100 nm and internal diameter of about 30–40 nm (they can be seen clearly in Fig. S1a), the lightweight hollow structure of PHCNF make itself more applicable for being an interlayer material. The hollow structure of PHCNF forms in the preparation process of polypyrrole (PPy) nanofibers

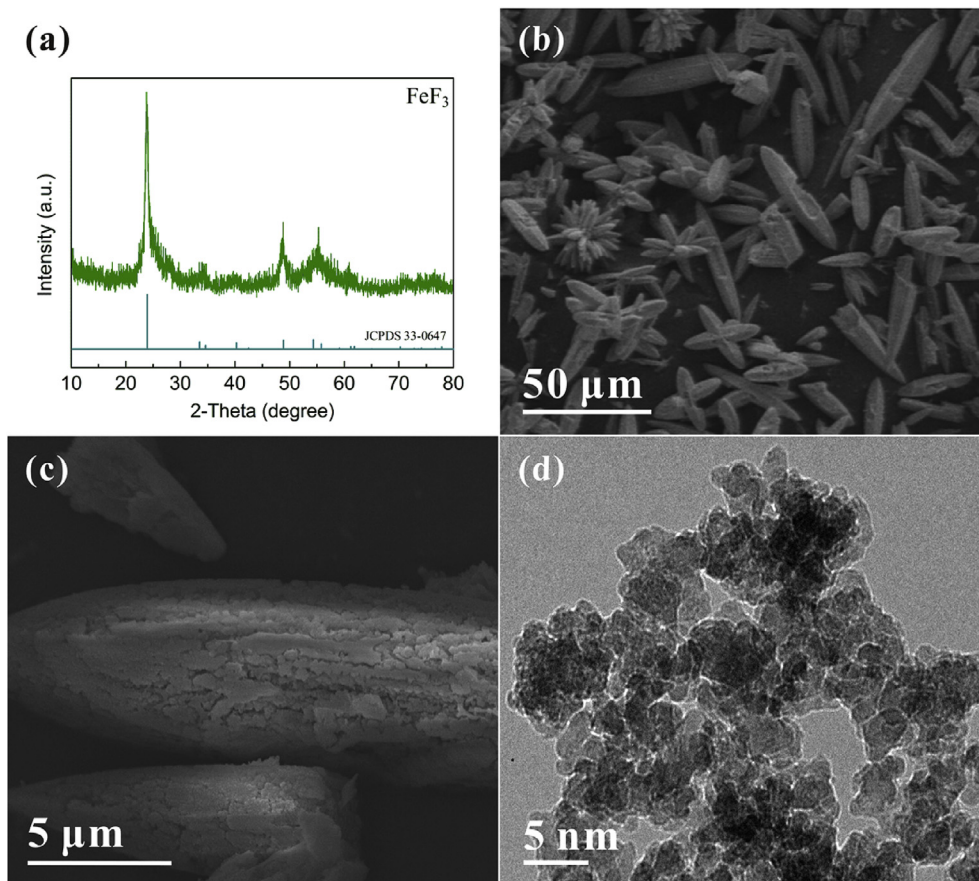


Fig. 1. X-ray diffraction (XRD) pattern (a), SEM images (b, c) and TEM image (d) of as-synthesized FeF_3 powders.

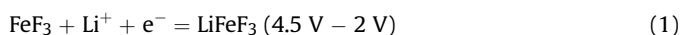
[42]. After carbonization, the hollow carbon nanofibers are achieved. In order to promote the adsorption capacity of the hollow carbon nanofibers, the subsequent activation of KOH makes the polypyrrole pyrolysis carbon nanofibers a unique porous one-dimensional nanostructure. The porous characteristics of PHCNF can be observed from the typical HRTEM image of PHCNF in Fig. S1b. Nitrogen adsorption desorption isotherms and pore size distribution patterns of PHCNF are shown in Fig. 2c, the nitrogen adsorption desorption isotherms depicts a typical type IV isotherms. The hysteresis loop indicates the existence of a micro-mesoporous hybrid structure [20]. The pore size distribution pattern, fitting from the corresponding absorption curve by BJH mode, suggests that most pores are smaller than 1.1 nm in diameter, and the average pore diameter is estimated to be 2.05 nm. The BET surface area of PHCNF is calculated to be $1404.38 \text{ m}^2 \text{ g}^{-1}$ with a total pore volume of $0.72 \text{ cm}^3 \text{ g}^{-1}$. The large specific surface area and porous structure are expected to strengthen the adsorption capacity and the electrolyte permeation of PHCNF.

It is reported that the presence of heteroatom at the carbon surface has a strong interatomic attraction, which can not only enhance electrical conductivity but also improve the adsorption ability of the carbons [43,44]. Fig. 2d shows the X-ray photoelectron spectroscopy spectra of PHCNF. It can be observed that three peaks centering at about 400.0, 285.0 and 532.0 eV corresponding to N1s, C1s and O1s, respectively, in the XPS survey spectrum of PHCNF [45]. The tests show the proportion of N in PHCNF is 2.24 wt %, the high-resolution N 1s spectrum of PHCNF is presented in Fig. 2d. The N 1s spectrum of PHCNF indicates that four different peaks, pyrrolic N located in a five-membered ring, pyridinic N located in a six-

membered ring, quaternary N, and other N, which are referred to as N - 5, N - 6, N - Q, and N - X. The four peaks can be identified at 400.36, 398.74, 401.45, and 403.20 eV, respectively. Thus the in-situ N-doped PHCNF is expected to be able to have certain adsorption ability, with its large specific surface area and good electrical conductivity [38,46].

Photographs illustrating the preparation process of FeF_3 cathode with PHCNF coating film are shown in Fig. 3a - b, PHCNF is uniformly coated onto the as-dried iron fluoride cathode with a scraper blade, a smooth surface is observed. Fig. 3c shows the cross-sectional image of electrode with PHCNF coating film, the thickness of the PHCNF film (PHCNF + PVDF) and the FeF_3 layer (FeF_3 + carbon black + PVDF) are about 3.5 μm and 26 μm , respectively. The weight of the PHCNF film and the FeF_3 layer is about 0.40 and 1.03 mg, which are determined by weighing the electrode before and after the coating process. That is, the PHCNF coating film accounted for about 27.9 wt% of the whole cathode (the PHCNF film and the FeF_3 layer). During the charge/discharge test, the mass of active material is calculated by the mass of FeF_3 in FeF_3 layer to be 0.72 mg. Fig. 3d shows the front-view image of PHCNF coating film, the porous and cross-linked network can be observed obviously.

Electrochemical performances of FeF_3 cathode materials with PHCNF coating film interlayer were investigated. It is widely considered that FeF_3 has high theoretical specific capacities of 237 mAh g^{-1} (2.0–4.5 V) and 712 mAh g^{-1} (1.5–4.5 V) by the following reactions [29–32]:



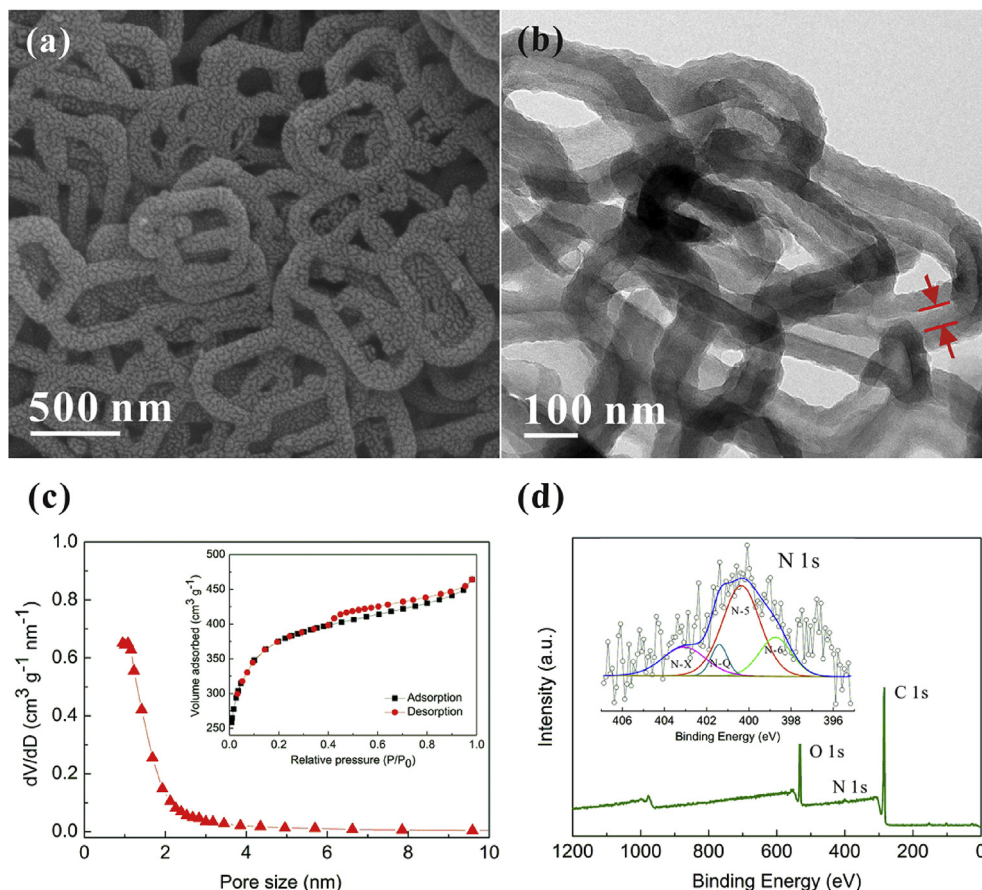
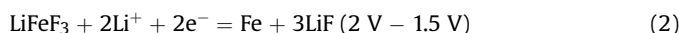


Fig. 2. Typical SEM (a) and TEM (b) images of PHCNF; Nitrogen adsorption-desorption isotherms and pore size distribution patterns of PHCNF (c); XPS spectrum for PHCNF with high-resolution spectrum for the N1s peaks (d).



Normally, Eq. (1) is ascribed to an intercalation reaction, FeF_3 maintain its original structure with the Li ion insertion during the reaction, and Equ. (2) represent a conversion reaction, which involves a structural change while cycling with the formation of zero-valent iron and LiF [19]. It is worth mentioning that LiF has the same insulating properties with FeF_3 , resulting in an obstacle for using the complete three-electron energy storage reaction. Fig. 4a - b show the cyclic voltammograms of FeF_3 cathode with PHCNF coating film and pure FeF_3 cathode without PHCNF coating film measured between 2.0 V and 4.5 V. As shown in Fig. 4a, there are two peaks in each reaction, and the cathodic and the anodic peak appear near 2.8 V and 3.2 V. In contrast, the cathodic and the anodic peaks appear near 2.1 V and 3.5 V in Fig. 4b. Their voltage differences are around 0.4 V and 1.4 V for the two samples, respectively, which indicates that the PHCNF coating film strengthen the kinetics of the electrochemical reaction obviously, and the large voltage hysteresis can be suppressed effectively. As shown in Figs. S2a–b, the similar results from CV tests can be observed while measuring in the 1.5–4.5 V region, further proving that the PHCNF coating film improve the reaction activity of the FeF_3 cathode obviously.

The cyclability and rate performance of the batteries were tested in various conditions to obtain a comprehensive evaluation for the role of PHCNF interlayer in improving electrochemical performance. Galvanostatic discharge-charge profiles were first performed in the 1.5–4.5 V region at 20 mA g^{-1} . The first charge and discharge capacities are about 594 and 536 mAh g^{-1} as shown in

Fig. S2c (corresponding voltage-capacity curves from the 1st to 3rd cycle can be seen in Fig. S2d), which do not measure up to the theoretical specific capacity of 712 mAh g^{-1} , this is likely due to that partial FeF_3 , with the poor electrical conductivity, was not involved in the electrode reaction. The pulverization of the FeF_3 cathode materials took place in the subsequent cycles, the discharge capacities are down to about 452 and 412 mAh g^{-1} , and after 20 cycles, the discharge capacity of 277 mAh g^{-1} is retained. The test results for the rate performance of the cells measured at 20–400 mA g^{-1} are demonstrated in Fig. S2e, a reversible capacity of about 196 and 134 mAh g^{-1} are achieved at 200 and 400 mA g^{-1} , respectively. After 35 cycles, the discharge capacity returns to 301 mAh g^{-1} at 20 mA g^{-1} . The relatively good test results of FeF_3 cathodes with the PHCNF coating film compared with pure FeF_3 cathodes benefits from the difunctional interlayer. Nevertheless, in the 1.5–4.5 V region, the voltage hysteresis is still serious and the capacity fades obviously in subsequent cycles, which result in serious energy loss.

Therefore, the same galvanostatic discharge-charge test was performed in the 2–4.5 V region. As shown in Fig. 4c, during the fore several cycles, a specific capacity of about 254 mAh g^{-1} was achieved at a current rate of 20 mA g^{-1} . This higher specific capacity than the theoretical specific capacity of 237 mAh g^{-1} is likely due to that partial FeF_3 participated in the reaction of Eq. (2). In the subsequent cycles, the interlayer enabled the FeF_3 cathode to retain an extremely high reversible specific capacity of about 217 mAh g^{-1} for 40 cycles, which is close to the theoretical specific capacity of 237 mAh g^{-1} . Fig. 4c also shows the corresponding specific energy

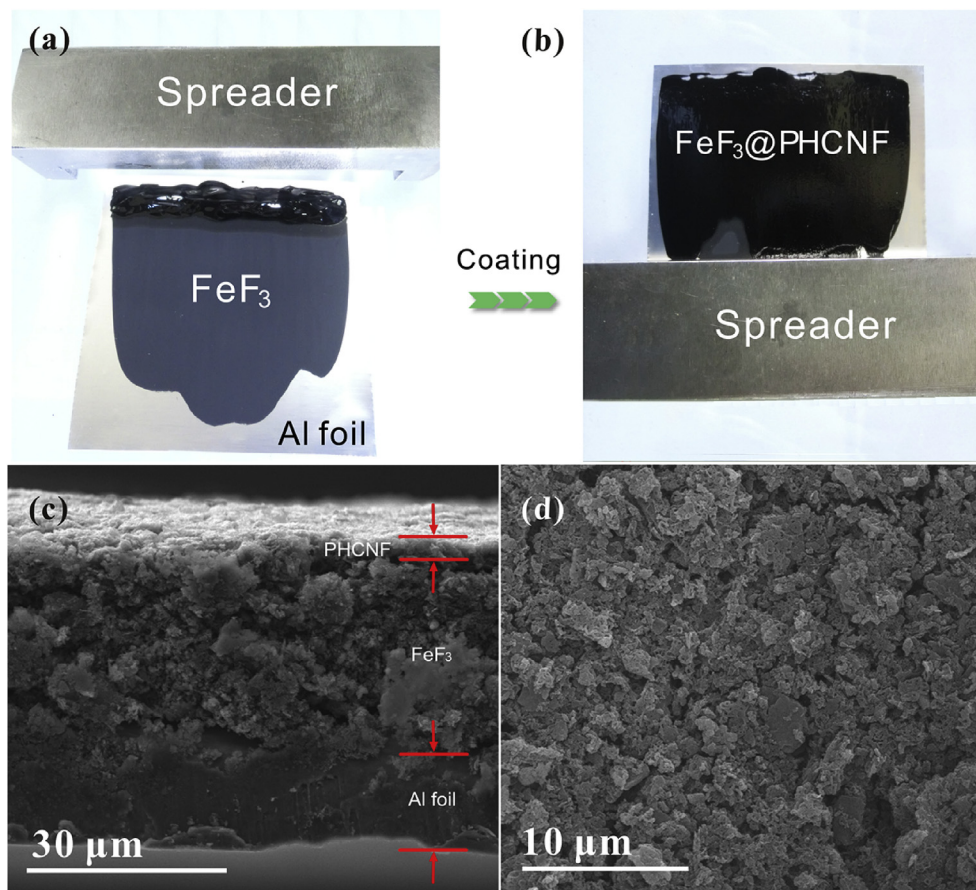


Fig. 3. Photographs of the coating process: as-prepared raw cathode (a) and double-layer cathode coated with PHCNF film (b); a typical cross-sectional SEM image of fresh cathode with PHCNF coating film (c) and a typical front-view SEM image of PHCNF coating film (d).

of FeF_3 cathode materials with interlayer of PHCNF coating film, the specific energy retained more than 612 Wh kg^{-1} , which is much higher than conventional cathode materials. Remarkably, the excellent specific capacity and energy are unprecedented, which are higher than the reported capacity under the same test conditions [22,23]. The parameters of electrochemical performance comparison with other studies are listed in Table S1. Fig. 4d shows the corresponding charge and discharge voltage-capacity curves from the 5th to 40th cycle at 20 mA g^{-1} , the coincident curves certified the outstanding cyclability of FeF_3 with the interlayer. Notably, the interlayer obviously improved the rate performance of FeF_3 cathode as well. As shown in Fig. 4e–f, the rate performance was measured at $20\text{--}1000 \text{ mA g}^{-1}$, under the high current rate condition, it can deliver close to 193 mAh g^{-1} at 200 mA g^{-1} . Meanwhile, superior capacities of $174, 123$ and 101 mAh g^{-1} were obtained at $400, 700$ and 1000 mA g^{-1} , respectively. Fig. 4f shows the corresponding discharge curves at different current densities. Obviously, the difunctional interlayer can obviously enhance electrochemical activity of FeF_3 cathode materials, which is widely considered as an insulating unsuitable material for cathode.

To further investigate the interfacial charge transfer in the “double-layer” electrode, electrochemical impedance spectra (EIS) were carried out at room temperature. Fig. 5a shows the typical Nyquist plots of FeF_3 cathode with interlayer before cycling and after cycling for 30 cycles, and pure FeF_3 cathode in Fig. 5b for comparison. It can be found that all Nyquist plots for these two types of electrodes consist of a single depressed semicircle in the high-to-medium frequency region relating to surface-film and

charge-transfer resistance ($R_{\text{sf+ct}}$), and an inclined line at low frequency relating to the ion transfer process [28,47]. An equivalent electrical circuit is used to fit the experimental impedance spectra as shown in Fig. 5c. Impedance parameters of FeF_3 cathode with PHCNF coating film and pure FeF_3 cathode without PHCNF coating film measured before cycling and after 30 cycles at different voltage are listed in Table 1. Impedance spectra of electrodes after 30 cycles are tested with a relaxation time of 30 min, and impedance spectra of lithium inserted electrodes are tested after another half cycle, when the voltage discharge to 2.0 V. Before cycling, the value of $R_{\text{sf+ct}}$ for FeF_3 cathode with interlayer is calculated to 28.8Ω . This value increases to 51.3Ω after 30 cycles at 4.5 V, which is mainly due to the structural change of the active material. $R_{\text{sf+ct}}$ testing at 2.0 V is lower than at 4.5 V, indicating that lithium-inserted FeF_3 has a better electronic conductivity. Also, it clearly shows that the values of $R_{\text{sf+ct}}$ for FeF_3 cathode with interlayer are much lower than that of pure FeF_3 under the same condition, which can prove that the one-dimensional N-doped PHCNF conductive interlayer significantly enhance the charge transfer rate of the electrode. After 30 cycles, the constant phase element capacitance values ($\text{CPE}_{\text{sf+ct}}$) at 2.0 V and 4.5 V of “double-layer” electrode are lower than that of pure FeF_3 electrode, also indicating an excellent charge transfer capacity of “double-layer” electrode. Therefore, the EIS data show that the strong interaction between the PHCNF and FeF_3 improves its own electrical conductivity and the “double-layer” electrode presents a superior charge transfer process enabling pure FeF_3 cathode to deliver extremely high specific capacity and excellent rate capability.

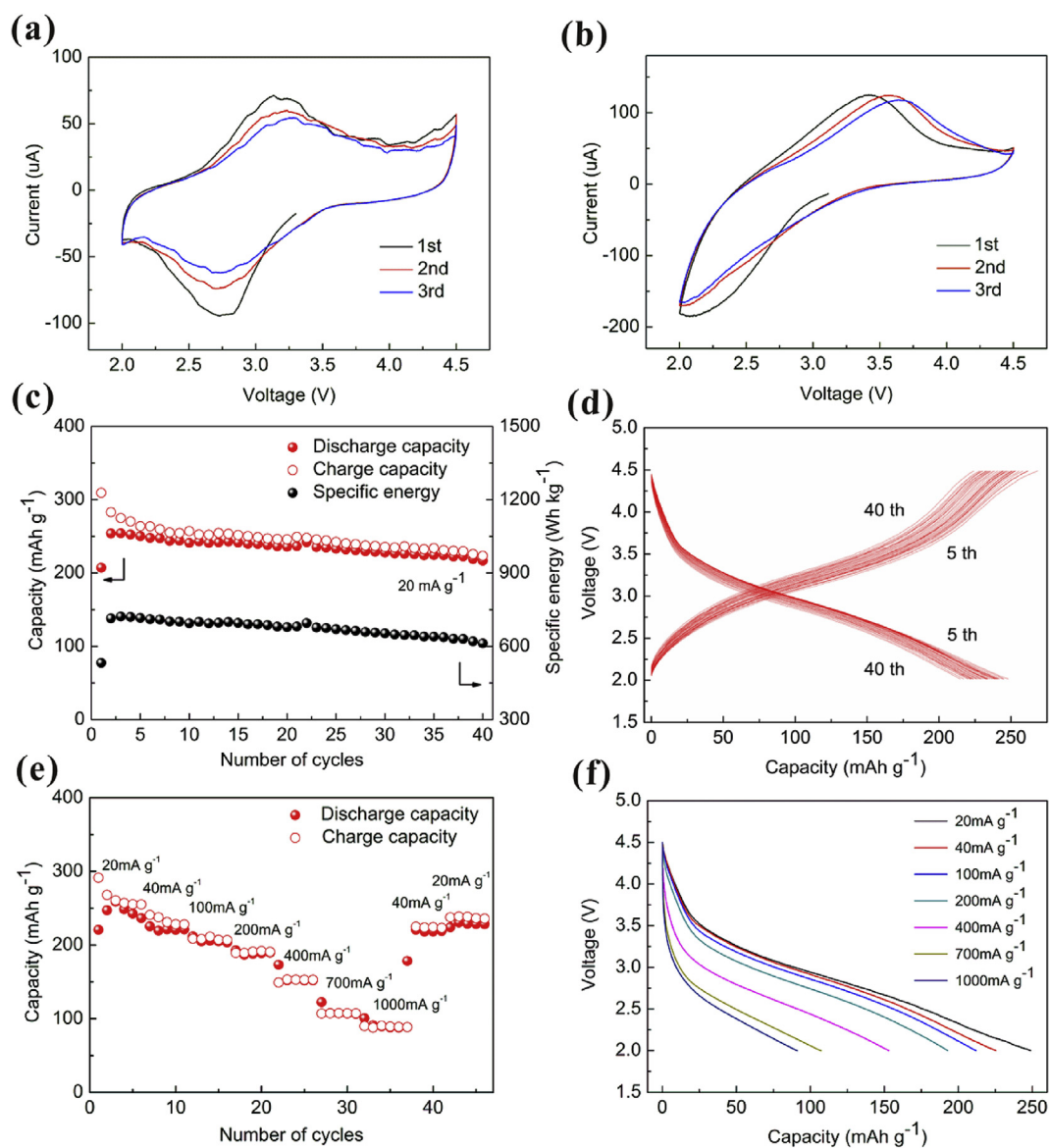


Fig. 4. Cyclic voltammograms of FeF_3 cathode with PHCNF coating film (a) and pure FeF_3 cathode without PHCNF coating film (b) measured at a voltage range of 2.0–4.5 V; Electrochemical performances of FeF_3 cathode materials with PHCNF coating film measured in the 2.0–4.5 V region: cycling performance at a current rate of 20 mA g^{-1} and corresponding specific energy (c); voltage-capacity curves at 20 mA g^{-1} for 35 cycles from the 5th to 40th cycle (d); Specific capacity at different current rates from 20 mA g^{-1} to 1000 mA g^{-1} (e); corresponding discharge profiles at different rates (f).

During the redox reaction of active materials, there is a large volume effect accompanying the structural changes, the bulk FeF_3 pulverizes into small particles, resulting in poor electrical conductivity and cyclability of FeF_3 . In order to investigate the function of the N-doped PHCNF coating film, Fig. 6a–c show the front-view images of the cathode with PHCNF coating film before cycling, after 45 and 100 cycles. Obvious changes occur on the surface of the electrode, a large number of nano-sized particles embedded on the surface of PHCNF with the increase of cycles as shown in Fig. 6b–c, it strongly indicates that the serious pulverization of electrodes exist indeed. After coated by PHCNF, by feat of the adsorption ability of the N-doped PHCNF, the escaped FeF_3 particles from the electrode are adsorbed in PHCNF surface. To reveal the element composition of the adsorbed particles, an energy dispersive spectrometer (EDS) analysis was performed on the surface of the PHCNF coating film. Fe and F signals are detected in the EDS result shown in Fig. 6d. Fig. 6e shows the elemental mapping of PHCNF coating

film cycled for 100 cycles. C, Fe and F signals are detected in the selected area. It implies that FeF_3 particles were evenly distributed on the surface of PHCNF after cycles. The SEM images, coupled with the EDS and elemental mapping results indicate that the interlayer of PHCNF coating film can effectively relieve the decay of the cyclability resulted from the pulverization of the FeF_3 cathode materials. The function of the interlayer can be ascribed into two points: On one hand, the trapped FeF_3 particles, adsorbed by the PHCNF, can be reactivated and continue to participate in reversible electrode reaction, on the other hand, the interconnected conductive network of PHCNF provides rapid electron transfer path to both the active materials left on the electrode and the trapped active materials particles.

4. Conclusions

In summary, an approach to enhance cycling performance of

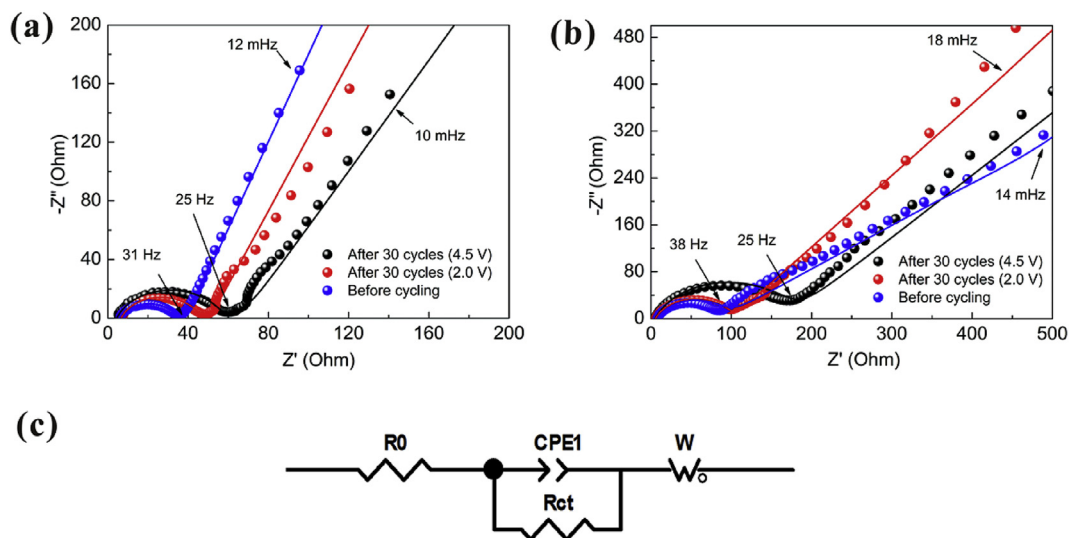


Fig. 5. EIS data of FeF_3 cathode with PHCNF coating film (a) and pure FeF_3 cathode without PHCNF coating film (b) measured before cycling and after 30 cycles at different voltage respectively; Equivalent electrical circuit used to fit the experimental impedance spectra (c).

Table 1
Impedance parameters of FeF_3 cathode with PHCNF coating film and pure FeF_3 cathode without PHCNF coating film measured before cycling and after 30 cycles at different voltage.

Sample	State	R_0/Ω	$R_{\text{sf+ct}}/\Omega$	$\text{CPE}_{\text{sf+ct}}/\mu\text{F}$
"double-layer" electrode	Before cycling (OCV 3.0 V)	5.4	28.8	20.9
	30 cycles (4.5 V)	4.3	51.3	7.8
	30 cycles (2.0 V)	6.5	38.6	8.6
Pure FeF_3 electrode	Before cycling (OCV 3.0 V)	7.4	79.5	18.4
	30 cycles (4.5 V)	4.8	166.4	11.8
	30 cycles (2.0 V)	5.4	94.6	14.5

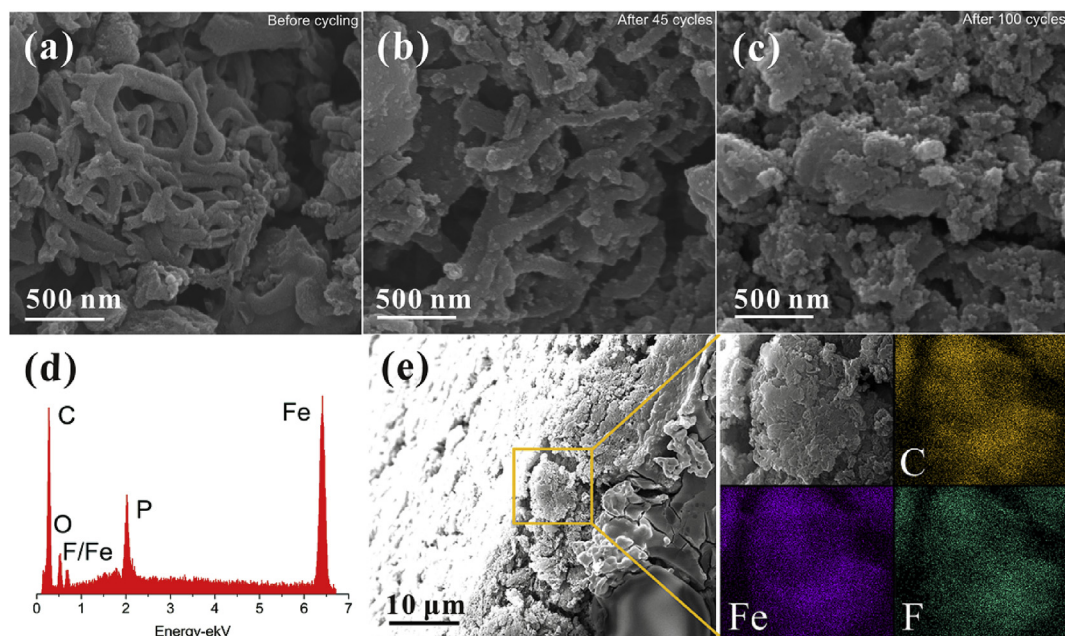


Fig. 6. Typical front-view SEM images of the cathode with PHCNF coating film: before cycling (a) and post-cycled characterization after 45 cycles (b) and 100 cycles (c) with its EDX spectrum (d); Elemental mapping of the PHCNF coating film cycled for 100 cycles (e).

pure FeF_3 cathode has been proposed simply by coating a light-weight N-doped porous hollow carbon nanofiber interlayer. The

difunctional interlayer composing of high conductive cross-linked carbon network not only provides an effective way to resolve the

problem of electrodes pulverization, but also improves the electrical conductivity of the FeF₃ cathode. The N-doped PHCNF interlayer enables the FeF₃ cathode achieve a superior electrochemical performance of enhanced specific capacity of about 217 mAh g⁻¹ at 20 mA g⁻¹ and rate performance delivering a high capacity of 193 and 101 mAh g⁻¹ at 200 mA g⁻¹ and 1000 mA g⁻¹ in the 2–4.5 V region. It is expected that the presented PHCNF interlayer in this paper may trigger more exploration in this direction to enhance the electrochemical performance of the conversion-type electrode materials for high-power Li rechargeable batteries.

Acknowledgements

This work was supported by the National Nature Science Foundation of China (no. 51204209 and 51274240), the Project of Innovation-driven Plan in Central South University and the Fundamental Research Funds for the Central Universities of Central South University (no. 2017zts122).

Appendix A. Supplementary data

Supplementary data related to this article can be found at <http://dx.doi.org/10.1016/j.jallcom.2017.06.266>.

References

- [1] B. Dunn, H. Kamath, J.M. Tarascon, Electrical energy storage for the grid: a battery of choices, *Science* 334 (2011) 928–935.
- [2] G. Liu, Development of a general sustainability indicator for renewable energy systems: a review, *Renew. Sustain. Energy Rev.* 31 (2014) 611–621.
- [3] Z.Q. Liu, A.X. Xu, Y.Y. Lv, X.X. Wang, Promoting the development of distributed concentrated solar thermal technology in China, *Renew. Sustain. Energy Rev.* 16 (2012) 1174–1179.
- [4] J. Hu, W. Li, Y. Duan, S. Cui, X. Song, Y. Liu, J. Zheng, Y. Lin, F. Pan, Single-particle performances and properties of LiFePO₄ nanocrystals for Li-ion batteries, *Adv. Energy Mater.* 7 (2017) 1601894.
- [5] K.S. Tan, M.V. Reddy, G.V.S. Rao, B.V.R. Chowdari, High-performance LiCoO₂ by molten salt (LiNO₃:LiCl) synthesis for Li-ion batteries, *J. Power Sources* 147 (2005) 241–248.
- [6] M.V. Reddy, S. Madhavi, G.V.S. Rao, B.V.R. Chowdari, Metal oxyfluorides TiOF₂ and NbO₂F as anodes for Li-ion batteries, *J. Power Sources* 162 (2006) 1312–1321.
- [7] M.V. Reddy, G.V.S. Rao, B.V.R. Chowdari, Metal oxides and oxysalts as anode materials for Li ion batteries, *Chem. Rev.* 113 (2013) 5364–5457.
- [8] A.S. Hameed, M.V. Reddy, N. Sarkar, B.V.R. Chowdari, J.J. Vittal, Synthesis and electrochemical investigation of novel phosphite based layered cathodes for Li-ion batteries, *Rsc Adv.* 5 (2015) 60630–60637.
- [9] M. Prabu, M.V. Reddy, S. Selvasekarapandian, G.V.S. Rao, B.V.R. Chowdari, Synthesis, impedance and electrochemical studies of lithium iron fluorophosphate, LiFePO₄F cathode, *Electrochim. Acta* 85 (2012) 572–578.
- [10] M. Nagarathinam, K. Saravanan, E.J.H. Phua, M.V. Reddy, B.V.R. Chowdari, J.J. Vittal, Redox-active metal-centered oxalato phosphate open framework cathode materials for lithium ion batteries, *Angew. Chem. Int. Ed. Engl.* 124 (2012) 5866–5870.
- [11] M.V. Reddy, G.V.S. Rao, B.V.R. Chowdari, Long-term cycling studies on 4 V-cathode, lithium vanadium fluorophosphate, *J. Power Sources* 195 (2010) 5768–5774.
- [12] S. Wei, X. Wang, M. Jiang, R. Zhang, Y. Shen, H. Hu, The FeF₃·0.33H₂O/C nanocomposite with open mesoporous structure as high-capacity cathode material for lithium/sodium ion batteries, *J. Alloys Compd.* 689 (2016) 945–951.
- [13] D.P. Opra, S.V. Gnedenkov, A.A. Sokolov, A.B. Podgorbunsky, N.M. Laptash, S.L. Sinebryukhov, Fluorine substituted molybdenum oxide as cathode material for Li-ion battery, *Mater. Lett.* 160 (2015) 175–178.
- [14] T. Erkert, Nanomaterials for lithium-ion batteries, *Russ. Chem. Rev.* 84 (2015) 826–852.
- [15] D. Sua, Y. Zhaoa, Y. Dong, C. Dinga, M. Ninga, J. Zhanga, J. Lia, H. Jina, Enhanced composites of V₂O₅ nanowires decorating on graphene layers as ideal cathode materials for lithium-ion batteries, *J. Alloys Compd.* 695 (2016) 2974–2980.
- [16] Y.L. Shi, M.F. Shen, S.D. Xu, X.Y. Qiu, L. Jiang, Y.H. Qiang, Q.C. Zhuang, S.G. Sun, Electrochemical impedance spectroscopic study of the electronic and ionic transport properties of NiF₂/C composites, *Int. J. Electrochem. Soc.* 6 (2011) 3399–3415.
- [17] Z.W. Fu, C.L. Li, W.Y. Liu, J. Ma, W. Ying, Q.Z. Qin, Z.W. Fu, C.L. Li, W.Y. Liu, J. Ma, Electrochemical reaction of lithium with cobalt fluoride thin film electrode, *J. Electrochem. Soc.* 152 (2005) E50–E55.
- [18] X. Hua, R. Robert, L.S. Du, K.M. Wiaderek, M. Leskes, K.W. Chapman, P.J. Chupas, C.P. Grey, Comprehensive study of the CuF₂ conversion reaction mechanism in a lithium ion battery, *J. Phys. Chem. C* 118 (2014) 15169–15184.
- [19] Y.H. Cui, M.Z. Xue, Y.N. Zhou, S.M. Peng, X.L. Wang, Z.W. Fu, The investigation on electrochemical reaction mechanism of CuF₂ thin film with lithium, *Electrochim. Acta* 56 (2011) 2328–2335.
- [20] H. Song, H. Cui, C. Wang, Extremely high-rate capacity and stable cycling of a highly ordered nanostructured carbon–FeF₂ battery cathode, *J. Mater. Chem. A* 3 (2015) 22377–22384.
- [21] M.A. Reddy, B. Breitung, V.S.K. Chakravadhanula, C. Wall, M. Engel, C. Kübel, A.K. Powell, H. Hahn, M. Fichtner, CF_x derived carbon–FeF₂ nanocomposites for reversible lithium storage, *Adv. Energy Mater.* 3 (2013) 308–313.
- [22] D. Ma, Z. Cao, H. Wang, X. Huang, L. Wang, X. Zhang, Three-dimensionally ordered macroporous FeF₃ and its in situ homogenous polymerization coating for high energy and power density lithium ion batteries, *Energy Environ. Sci.* 5 (2012) 8538–8542.
- [23] S.W. Kim, D.H. Seo, H. Gwon, J. Kim, K. Kang, Fabrication of FeF₃ nanoflowers on CNT branches and their application to high power lithium rechargeable batteries, *Adv. Mater.* 22 (2010) 5260–5264.
- [24] F. Badway, N. Pereira, F. Cosandey, G.G. Amatucci, Carbon-metal fluoride nanocomposites structure and electrochemistry of FeF₃:C, *J. Electrochem. Soc.* 150 (2003) A1209–A1218.
- [25] F. Badway, F. Cosandey, N. Pereira, G.G. Amatucci, Carbon metal fluoride nanocomposites high-capacity reversible metal fluoride conversion materials as rechargeable positive electrodes for Li batteries, *J. Electrochem. Soc.* 150 (2003) A1318–A1327.
- [26] F. Cosandey, J.F. Alsharab, F. Badway, G.G. Amatucci, P. Stadelmann, EELS spectroscopy of iron fluorides and FeF_x/C nanocomposite electrodes used in Li-ion batteries, *Microsc. Microanal. Off. J. Microsc. Soc. Am. Microbeam Anal. Soc. Microsc. Soc. Can.* 13 (2007) 87–95.
- [27] A. Sakunthala, M.V. Reddy, S. Selvasekarapandian, B.V.R. Chowdari, P.C. Selvin, Preparation, characterization, and electrochemical performance of lithium trivanadate rods by a surfactant-assisted polymer precursor method for lithium batteries, *J. Phys. Chem. C* 114 (2010) 8099–8107.
- [28] A. Sakunthala, M.V. Reddy, S. Selvasekarapandian, B.V.R. Chowdari, P.C. Selvin, Energy storage studies of bare and doped vanadium pentoxide, (V_{1.95}M_{0.05})O₅, M = Nb, Ta, for lithium ion batteries, *Energy & Environ. Sci.* 4 (2011) 1712–1725.
- [29] F. Wang, R. Robert, N.A. Chernova, N. Pereira, F. Omenya, F. Badway, X. Hua, M. Ruotolo, R. Zhang, L. Wu, Conversion reaction mechanisms in lithium ion batteries: study of the binary metal fluoride electrodes, *J. Am. Chem. Soc.* 133 (2011) 18828–18836.
- [30] N. Yamakawa, M. Jiang, B. Key, C.P. Grey, Identifying the local structures formed during lithiation of the conversion material, iron fluoride, in a Li ion battery: a solid-state NMR, X-ray diffraction, and pair distribution function analysis study, *J. Am. Chem. Soc.* 131 (2009) 10525–10536.
- [31] R. Prakash, C. Wall, A.K. Mishra, C. Kübel, M. Ghafari, H. Hahn, M. Fichtner, Modified synthesis of [Fe/LiF/C] nanocomposite, and its application as conversion cathode material in lithium batteries, *J. Power Sources* 196 (2011) 5936–5944.
- [32] L. Li, F. Meng, S. Jin, High-capacity lithium-ion battery conversion cathodes based on iron fluoride nanowires and insights into the conversion mechanism, *Nano Lett.* 12 (2012) 6030–6037.
- [33] J. Liu, Y. Wan, W. Liu, Z. Ma, S. Ji, J. Wang, Y. Zhou, P. Hodgson, Y. Li, Mild and cost-effective synthesis of iron fluoride-graphene nanocomposites for high-rate Li-ion battery cathodes, *J. Mater. Chem.* 1 (2013) 1969–1975.
- [34] Y. Bai, X. Zhou, Z. Jia, C. Wu, L. Yang, M. Chen, H. Zhao, F. Wu, G. Liu, Understanding the combined effects of microcrystal growth and band gap reduction for Fe_(1-x)Ti_xF₃ nanocomposites as cathode materials for lithium-ion batteries, *Nano Energy* 17 (2015) 140–151.
- [35] J. Yang, Z. Xu, H. Sun, X. Zhou, A three-dimensional interlayer composed of graphene and porous carbon for Long-life, High capacity Lithium-Iron Fluoride Battery, *Electrochim. Acta* 220 (2016) 75–82.
- [36] Z. Xiao, Z. Yang, L. Wang, H. Nie, M. Zhong, Q. Lai, X. Xu, L. Zhang, S. Huang, Lithium-Sulfur batteries: a lightweight TiO₂/graphene interlayer, applied as a highly effective polysulfide absorbent for fast, long-life lithium-sulfur batteries (Adv. Mater. 18/2015), *Adv. Mater.* 27 (2015) 2890.
- [37] L. Qie, W.M. Chen, Z.H. Wang, Q.G. Shao, X. Li, L.X. Yuan, X.L. Hu, W.X. Zhang, Y.H. Huang, Nitrogen-doped porous carbon nanofiber webs as anodes for lithium ion batteries with a superhigh capacity and rate capability, *Adv. Mater.* 24 (2012) 2047–2050.
- [38] J. Yang, J. Xie, X. Zhou, Y. Zou, J. Tang, S. Wang, F. Chen, L. Wang, Functionalized N-Doped porous carbon nanofiber webs for a lithium-sulfur battery with high capacity and rate performance, *J. Phys. Chem. C* 118 (2014) 1800–1807.
- [39] Y.-L. Shi, N. Wu, M.-F. Shen, Y.-L. Cui, L. Jiang, Y.-H. Qiang, Q.-C. Zhuang, Electrochemical behavior of iron(III) fluoride trihydrate as a cathode in lithium-ion batteries, *Chemelectrochem* 1 (2014) 645–654.
- [40] G. Ali, S.H. Oh, S.Y. Kim, J.Y. Kim, B.W. Cho, K.Y. Chung, An open-framework iron fluoride and reduced graphene oxide nanocomposite as a high-capacity cathode material for Na-ion batteries, *J. Mater. Chem. A* 3 (2015) 10258–10266.
- [41] B. Li, Z. Cheng, N. Zhang, K. Sun, Self-supported, binder-free 3D hierarchical iron fluoride flower-like array as high power cathode material for lithium batteries, *Nano Energy* 4 (2014) 7–13.

- [42] Y. Shen, M. Wan, Tubular polypyrrole synthesized by in situ doping polymerization in the presence of organic function acids as dopants, *J. Polym. Sci. Part A Polym. Chem.* 37 (1999) 1443–1449.
- [43] G. Wu, C. Dai, D. Wang, D. Li, N. Li, Nitrogen-doped magnetic onion-like carbon as support for Pt particles in a hybrid cathode catalyst for fuel cells, *J. Mater. Chem.* 20 (2010) 3059–3068.
- [44] F. Su, C.K. Poh, J.S. Chen, G. Xu, D. Wang, Q. Li, J. Lin, X.W. Lou, Nitrogen-containing microporous carbon nanospheres with improved capacitive properties, *Energy & Environ. Sci.* 43 (2011) S229–S236.
- [45] Y.S. Su, A. Manthiram, A new approach to improve cycle performance of rechargeable lithium-sulfur batteries by inserting a free-standing MWCNT interlayer, *Chem. Commun.* 48 (2012) 8817–8819.
- [46] X. Zhou, J. Tang, J. Yang, J. Xie, B. Huang, Seaweed-like porous carbon from the decomposition of polypyrrole nanowires for application in lithium ion batteries, *J. Mater. Chem. A* 1 (2013) 5037–5044.
- [47] M.V. Reddy, G.V.S. Rao, B.V.R. Chowdari, Nano-(VSbSn)O : a high capacity, high rate anode material for Li-ion batteries, *J. Mater. Chem.* 21 (2011) 10003–10011.